

# Development of Nanoparticle-Stabilized Foams to Improve Performance of Water-less Hydraulic Fracturing

*Masa Prodanovic*

CONTRACT NO. DE- FE0013723

## FINAL TECHNICAL REPORT

**Original Project Period: 1 Oct 2013 – 30 Sept 2016**

**Extension Period: 1 Oct 2017 – 30 Sept 2017**

**December 29, 2017**

*Prepared by*

**Maša Prodanović (PI)**

Department of Petroleum and Geosystems Engineering

The University of Texas at Austin

200 E. Dean Keeton, Stop C0300

Austin, TX 78712-0228

Phone: (512) 471 0839

Email: [masha@utexas.edu](mailto:masha@utexas.edu)

DUNS: 170230239

and

**Keith P. Johnston (co-PI)**

Department of Chemical Engineering

The University of Texas at Austin

Phone: (512) 471 4617

Email: [johnston@che.utexas.edu](mailto:johnston@che.utexas.edu)

*Prepared for*

**U.S. Department of Energy - NETL**

3610 Collins Ferry Road, P.O. Box 880,

Morgantown, WV 26508

Acknowledgment: "This material is based upon work supported by the Department of Energy under Award Number DE-FE0013723."

Disclaimer: "This report was prepared as an account of work sponsored by an agency of the United States Government. Neither the United States Government nor any agency thereof, nor any of their employees, makes any warranty, express or implied, or assumes any legal liability or responsibility for the accuracy, completeness, or usefulness of any information, apparatus, product, or process disclosed, or represents that its use would not infringe privately owned rights. Reference herein to any specific commercial product, process, or service by trade name, trademark, manufacturer, or otherwise does not necessarily constitute or imply its endorsement, recommendation, or favoring by the United States Government or any agency thereof.

The views and opinions of authors expressed herein do not necessarily state or reflect those of the United States Government or any agency thereof.

## **1. Abstract**

We have successfully created ultra dry CO<sub>2</sub>-in-water and N<sub>2</sub>-in-water foams (with water content down to 2-5% range), that are remarkably stable at high temperatures (up to 120 deg, C) and pressures (up to 3000psi) and viscous enough (100-200 cP tunable range) to carry proppant. Two generations of these ultra-dry foams have been developed; they are stabilized either with a synergy of surfactants and nanoparticle, or just with viscoelastic surfactants that viscosify the aqueous phase. Not only does this reduce water utilization and disposal, but it minimizes fluid blocking of hydrocarbon production. Further, the most recent development shows successful use of environmentally friendly surfactants at high temperature and pressure. We pay special attention to the role of nanoparticles in stabilization of the foams, specifically for high salinity brines. The preliminary numerical simulation for which shows they open wider fractures with shorter half-length and require less clean-up due to minimal water use. We also tested the stability and sand carrying properties of these foams at high pressure, room temperature conditions in sapphire cell. We performed on a preliminary numerical investigation of applicability for improved oil recovery applications. The applicability was evaluated by running multiphase flow injection simulations in a case-study oil reservoir. The results of this research thus expand the options available to operators for hydraulic fracturing and can simplify the design and field implementation of foamed fracturing fluids.

## Table of Contents

<b>1. Abstract .....</b>	<b>2</b>
<b>2. Executive Summary .....</b>	<b>4</b>
<b>3. Experimental Methods .....</b>	<b>6</b>
<b>4. Results and discussion .....</b>	<b>10</b>
4.1. Key technology for foam stabilization .....	10
4.2 Foams stabilized with NPs, surfactant and polymer (“the first generation”) .....	10
4.3 Foams stabilized with viscoelastic surfactants .....	16
4.4. Nitrogen-in-water foams (unpublished) .....	18
4.5 Further study on the effect of nanoparticles in foam (unpublished).....	20
4.6. Publications from this work.....	24
<b>5 Conclusions .....</b>	<b>25</b>
<b>6 List of Figures .....</b>	<b>26</b>
<b>7 List of Tables .....</b>	<b>27</b>
<b>8 References .....</b>	<b>27</b>

## 2. Executive Summary

**Motivation.** Foamed fluids have been used for hydraulic fracturing for more than 40 years [1], [2]. The list of advantages of foamed fracturing fluid is that they: (1) add energy to the fluid via addition of a compressible gas which improves flowback of the treatment and enhances subsequent production rates; (2) have lower liquid content which reduces fluid losses to the formation and fluid damage to water-sensitive formations; and (3) have higher viscosities which improves sand-carrying and sand-suspending properties and creates wider fractures. The implication of (2) is also that foam *fracturing fluids use less water*. This may prove decisive for continued development of unconventional oil and gas (UOG) resources which require growing number of wells as well as fracturing stage per horizontal well, despite the added upfront cost of bringing gas (e.g. carbon dioxide or nitrogen) to the well location. Indeed, UOG development is responsible for maintaining gas production rates in the US over the last twenty years, for increasing US gas production in the last few years, and for reversing the decades-long declines in US oil production over the last five years. This trend of rising domestic hydrocarbon production is remarkable and has broad economic and policy implications. The most contentious of these implications is the role of water.

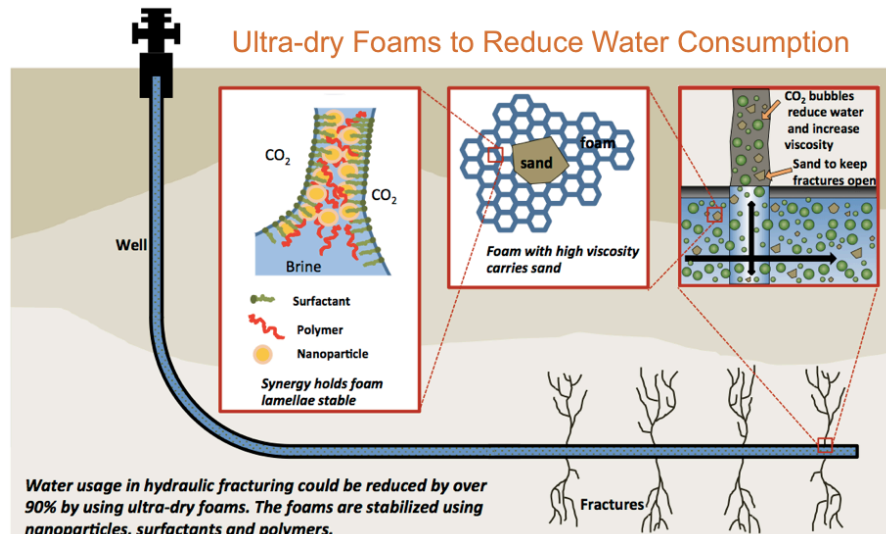


**Figure 1** The overview of the synergy required for stabilization of ultradry foams as well as their intended usage in hydraulic fracturing. Ultradry foams are defined as foams with volumetric gas content, or quality, of 90% and above.

We started this project with the aim of creating technology that enables minimizing or even eradicating the water content in fracturing fluids (Figure 1). Historically, fracturing fluids have been formulated with fresh water, and in most applications the water content is typically 25-90% (by volume). Unfortunately, in some UOG locations water is already scarce, and competition for it pits multiple sectors of the economy and of the community against each other. Further, the injected fluid is either lost to the formation or is returned to the surface where it needs to be treated and/or re-injected. In all UOG locations the recovery, treatment and discharge/disposal of flowback water from large-scale development presents economic and environmental challenges. All forecasts for UOG indicate that these problems will only grow. As a result, the US faces a serious dilemma: should water resources be used to enable domestic oil and gas production, or should resurgent hydrocarbon production be restricted or even prevented so that water remains available for other uses?

CO<sub>2</sub>/water and N<sub>2</sub>/water foams are also of interest for mobility control in CO<sub>2</sub> enhanced oil recovery (EOR) and as energized fracture fluids, or in hybrid processes that combine aspects of both processes. In fracturing applications, it would be desirable to find ways to lower the water level as much as possible to

minimize the production of wastewater and prevent formation damage. However, it is challenging to stabilize ultradry foams with extremely high internal phase gas fraction given the high capillary pressure and the rapid drainage rate of the lamellae between the gas bubbles.

**Achievements.** We have successfully created ultra dry CO<sub>2</sub>-in-water foams (with water content down to 2-5% range) as well as similar nitrogen-in-water foams, that are remarkably stable at high temperatures (up to 120 deg. C) and pressures (up to 3000psi) and viscous enough (100-200 cP tunable range) to carry proppant. Such ultradry foams (at close to reservoir conditions) are fairly new science, and the schematic in

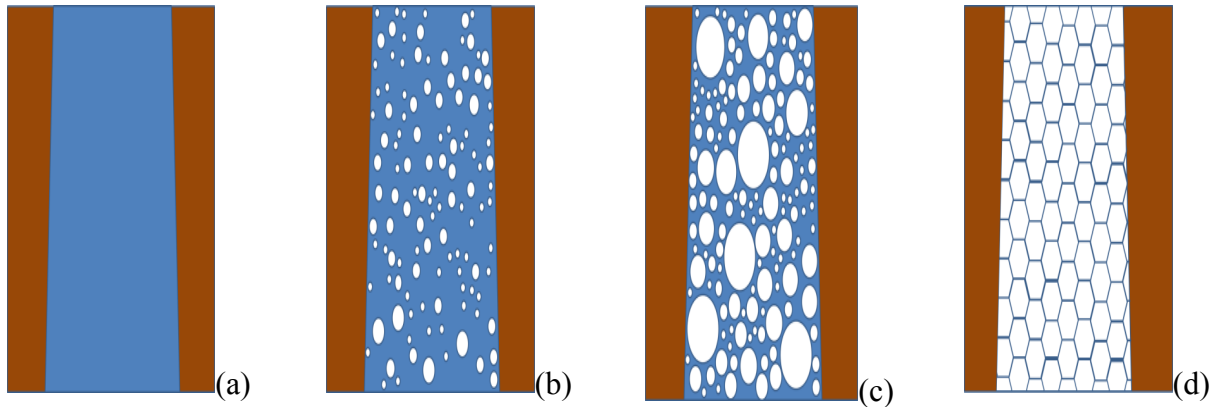
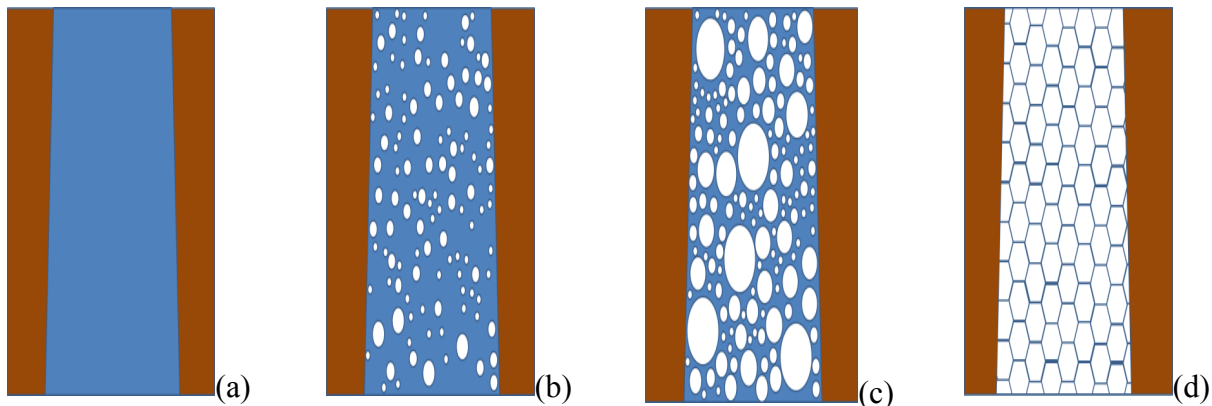


Figure 2 shows the relative difference in their water/gas content compared to common fracturing fluids. Two generations of these ultra-dry foams have been developed; they are stabilized either with a synergy of surfactants and nanoparticles [3], or just with viscoelastic surfactants [4] that viscosify the aqueous phase. Not only does this reduce water utilization and disposal, but it minimizes fluid blocking of hydrocarbon production. Further, the most recent development shows successful use of environmentally friendly surfactants at high temperature and pressure [5]. The preliminary numerical simulation for which shows they open wider fractures with shorter half-length [6] and require less clean-up due to minimal water use. Table 1 below summarizes the type of surfactants, polymers and/or nanoparticles used in these developments.



**Figure 2 Schematic of ultradry foams gas content vs. the hydraulic fracturing fluids currently in use (a) water, (b) energized fluids (gas content  $Q \sim 0.3$ ), (c) foam ( $Q \sim 0.6$ ), and (d) ultrdry foam ( $Q > 0.9$ ).**

We also tested the stability and sand carrying properties of these foams at high pressure, room temperature conditions in sapphire cell [7]. In the same work we performed on a preliminary numerical investigation of applicability for improved oil recovery applications. The applicability was evaluated by running multiphase flow injection simulations in a case-study oil reservoir. We finally repeat very similar

results for nitrogen-in-foam results and specifically investigate the role of nanoparticles in stabilization of foams in presence of high salinity brines (both unpublished work).

The results of this research thus expand the options available to operators for hydraulic fracturing and can simplify the design and field implementation of foamed frac fluids. Since development of these high-quality-highly-stable foams for subsurface applications is fairly new science, they have been only generated and tested using sand packs and porous cores in lab scale. Note that parallel DOE sponsored research (DE-FE0024314, [8]) has been developing the necessary topside infrastructure for generating natural gas based foams and injecting them in the field, but has not tested ultradry foams. The technology will make it easier for operators to switch to reduced-water or zero-water hydraulic fracturing campaigns, thereby alleviating one of the most sensitive challenges for domestic hydrocarbon production.

### 3. Experimental Methods

**Materials.** Table 1 summarizes the surfactant and nanoparticle materials/systems used in our published studies for carbon-dioxide-in-water ultradry foams, including the range of conditions at which they are stable as well as main properties measured on them. The referenced papers have more details on the materials, and the sections below detail how the property measurements were performed.

**Table 1. Summary of ultra dry CO<sub>2</sub>/water foam systems. These are representative systems rather than an exhaustive list (please refer to publications).**

System	Salt	Pressure (Psig)	Temp. (°C)	Shear rate/s	Quality (%)	Viscosity (cP)	Source
1% OAPB (Oleyl dimethyl amidopropyl betaine)	2% KCl*	3000	90	200	98	103	[5]
1% EDAB (erucyl dimethyl amidopropyl betaine)	2% KCl*	3000	90	200	95	90	[5]
3.6%SLES+0.4% C10DMA (N,N-Dimethyl-n-decylamine)	2% KCl*	3000	RT	200	95	184	[4]
3.6% SLES (Sodium Lauryl ether sulfate)	2% KCl*	3000	RT	200	95	145	[4]
0.88%HPAM+0.08%LAPB (Lauryl amidopropyl betaine) +1% silica nanoparticles	2%KCl	3000	50	200	0.9	230	[3]
0.88% HPAM+0.08% LAPB	2%KCl	3000	50	200	0.9	90	[3]

\*Can work at higher salt conc. as well.

**High Pressure CO<sub>2</sub>/Water Interfacial Tension Measurements.** The interfacial tension between CO<sub>2</sub> and water at 3000 psia was determined at room temperature using from axisymmetric drop shape analysis of a pendant CO<sub>2</sub> bubble, where equipment and techniques were adapted from previous studies. Pendant CO<sub>2</sub> bubbles were formed at the end of a stainless steel capillary (1.59 mm O.D x 0.50 mm I.D.) in the variable-volume view cell containing 16 mL of aqueous phase with a known concentration of surfactant and/or nanoparticles.

Prior to the formation of pendant bubbles, the aqueous phase was stirred for 2 h in the presence of excess CO<sub>2</sub> to saturate the aqueous phase. The typical size of the bubble was 2–4 mm in diameter. Bubbles were equilibrated for 10 min. prior to imaging. The density of the aqueous brine phase was determined by assuming ideal mixing between CO<sub>2</sub> at a density of 1 g/cm<sup>3</sup> and the brine density (containing surfactant) of 1.3 g/cm<sup>3</sup>. The mean interfacial tension from at least 3 bubbles is reported. More details are available in [3].

**Rheology Measurements.** Shear viscosity at steady state and room temperature for aqueous dispersions of nanoparticles and surfactants was characterized using AR G2 rotational rheometer (TA Instruments) equipped with a cone-and-plate geometry. The pH of the aqueous dispersions was adjusted with 1 N HCl or NaOH to be 3.5. At least 3 scans of shear rates were performed for each aqueous dispersion and the reported values represent average values. The variation for multiple measurements was within 10%. Oscillatory measurements were carried out with a frequency sweep between 1 rad/s to 400 rad/s. The rotational rheometer was used in the strain controlled mode with strain amplitude of 5%, which was in the linear viscoelasticity-region for the measurements. A sinusoidal strain was applied and the torque induced by the resulting shear stress was measured to obtain the dynamic storage and loss modulus. More details are available in [3].

**Surface Shear Viscosity Measurements.** Surface shear viscosity at steady state between air and 2% KCl aqueous dispersions containing surfactants and nanoparticles at room temperature and pH 3.5 was measured using AR G2 rotational rheometer (TA Instruments) equipped with double wall ring (DWR) geometry. Detailed information of the DWR geometry was described by Vanderbril et al.<sup>44</sup> The ring was carefully placed at the air-water interface as indicated by the capillary rise. The measured steady state torque at angular velocity of 1 rad/s was averaged over at least 6 measurements. The relative contribution of the bulk sub-phase drag and surface drag to the measured steady state torque was evaluated with the dimensionless Boussinesq number, defined as:

$$Bo = \frac{\text{surface drag}}{\text{subphase drag}} = \frac{\mu_s \frac{V}{L_b} P_l}{\mu \frac{V}{L_s} A_s} = \frac{\mu_s}{\mu_b G} \quad (1)$$

where  $\mu_s$  is the surface shear viscosity (Pa s m),  $\mu_b$  is the viscosity of the bulk sub-phase (Pa s),  $V$  is the characteristic velocity,  $L_b$  and  $L_s$  are the characteristic length scales over which the velocity decays at the bulk sub-phase and surface, respectively,  $P_l$  is the perimeter of the concentric annular circles at contact, and  $A_s$  is the contact area of the ring and the surface (i.e. the annular area), respectively.<sup>44</sup>  $G$  is the characteristic length of the DWR geometry (0.7 mm). The measured apparent surface viscosity was corrected with an iterative numerical procedure. Surface viscosity after the correction of sub-phase drag following the procedures described by Vanderbril et al.<sup>44</sup> was reported in this study. More details are available in [3].

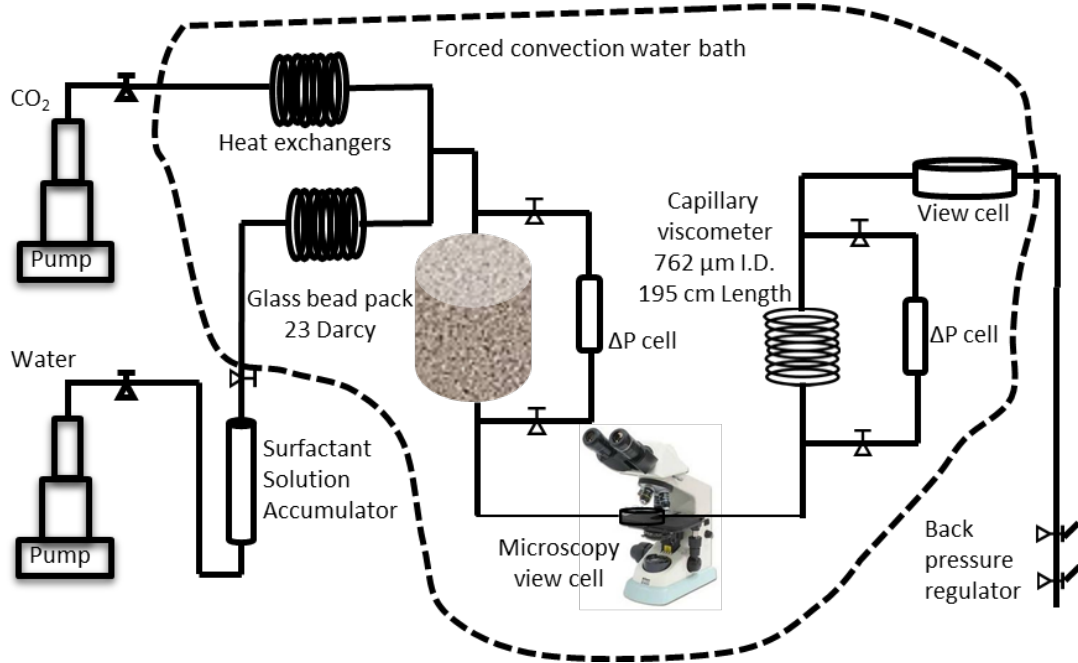


**Figure 3. Schematic of the apparatus used for apparent foam viscosity and mean bubble size measurements. A glass bead pack was used as the foam generator.**

**CO<sub>2</sub>/Water Foam Formation and Viscosity.** C/W foam viscosity under high pressure was measured with the flow system shown in Figure 3.<sup>7,16</sup> Before injection of CO<sub>2</sub>, twenty pore volumes of aqueous dispersion (40 mL) were injected through the beadpack (pore volume = 0.45 mL) to obtain saturation. The glass bead pack had an inner diameter of 0.38 cm and length of 11.3 cm, packed with 180 μm spherical glass beads (70-100 mesh soda-lime silica glass, stock number P-0080, Potters Industries Inc., Valley Forge, PA). The pore throat size in the glass bead pack ranged from 28 to 75 μm for hexagonally and cubic packed of 180 μm spheres, respectively. The foam flowed into a high pressure view cell<sup>7</sup> where the macroscopic appearance could be visually observed. The apparent viscosity of foam ( $\mu_{app}$ ) was measured from the  $\Delta P/\Delta L$  across the capillary tube of length  $L$  (195 cm) with the Hagen–Poiseuille equation for a Newtonian fluid in laminar flow:

$$\mu_{app} = \frac{\pi \cdot \Delta P \cdot R^4}{8 \cdot q \cdot L} \quad (2)$$

where  $R$  is the inner radius of the capillary tube (381 μm) and  $q$  is the volumetric flow rate. The foam was generated in the glass bead pack at a superficial velocity of 200 ft/day, yielding a wall shear rate of 200 s<sup>-1</sup> at the capillary tube, and residence time of 54 s and 107 s in the glass bead pack and the capillary tube, respectively. More details are available in [3].

**CO<sub>2</sub>/Water Foam Morphology and Stability.** Micrographs of foam bubbles were captured at room temperature *in situ* with a high pressure microscopy cell installed at the exit of the glass bead pack. The microscopy cell was mounted onto a microscope (Nissan Eclipse ME600). The sapphire windows (Swiss Jewel Company, W6.36, 0.635 cm diameter and 0.229 cm thickness) were separated by Teflon spacers, allowing observation of foam with a 10 × magnification objective lens, giving minimum measurable bubble size of 1.8 μm. At least 100

bubbles were analysed to show the mean bubble size and size distributions. The Sauter mean diameter  $D_{sm}$  and the dimensionless polydispersity  $U_{poly}$  of foam bubbles are calculated as follows:

$$D_{sm} = \frac{\sum_i D_i^3}{\sum_i D_i^2} \quad (3)$$

$$U_{poly} = \frac{1}{D_{med}} \frac{\sum_i D_i^3 |D_{med} - D_i|}{\sum_i D_i^3} \quad (4)$$

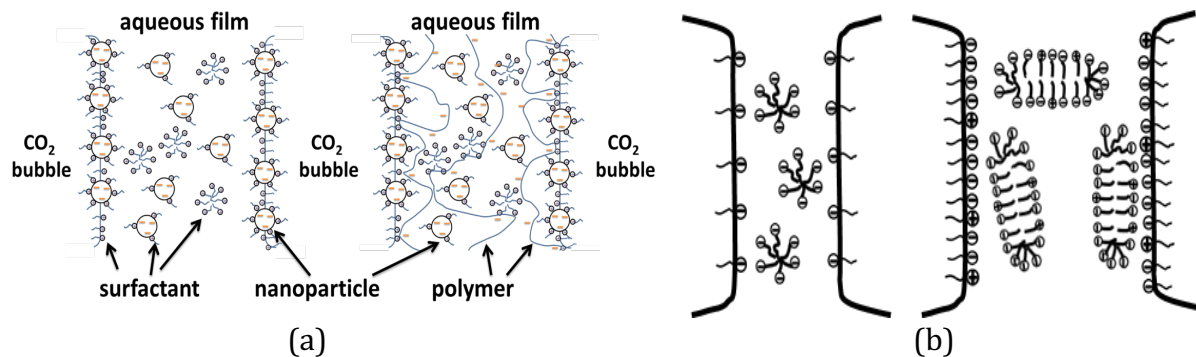
where  $D_i$  is the diameter of a foam bubble,  $D_{med}$  is the volume averaged median diameter of bubbles. More details are available in [3].

**Air-Water Lamella Thickness Measurements.** The Zeiss LSM 710/Elyra S.1 confocal microscope equipped with structured illumination super resolution system was used to measure the aqueous lamella thickness of the air-water foams.

## 4. Results and discussion

### 4.1. Key technology for foam stabilization

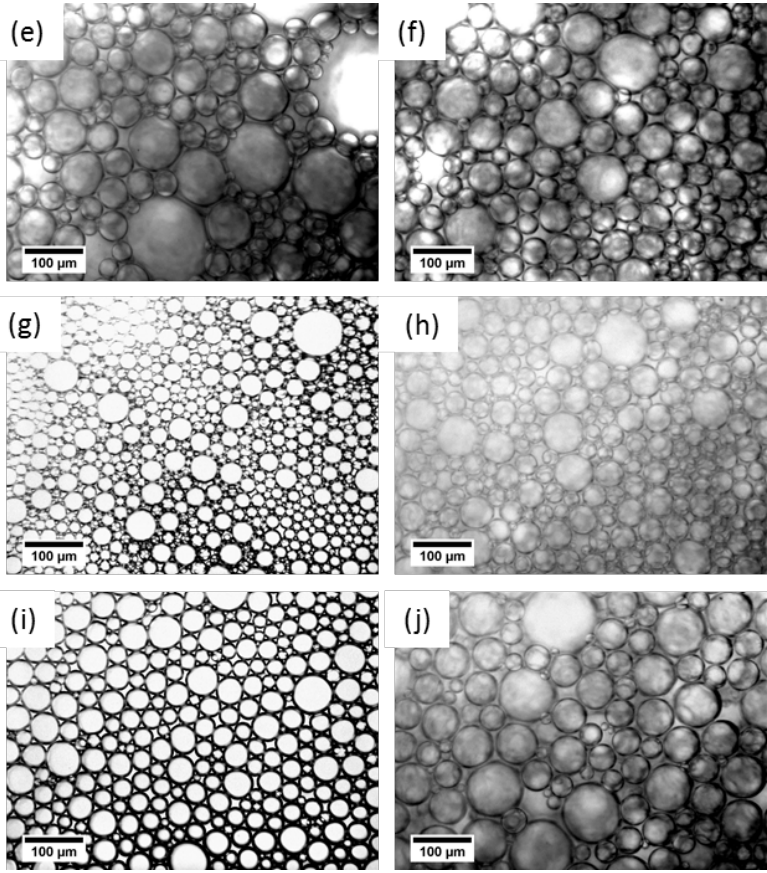
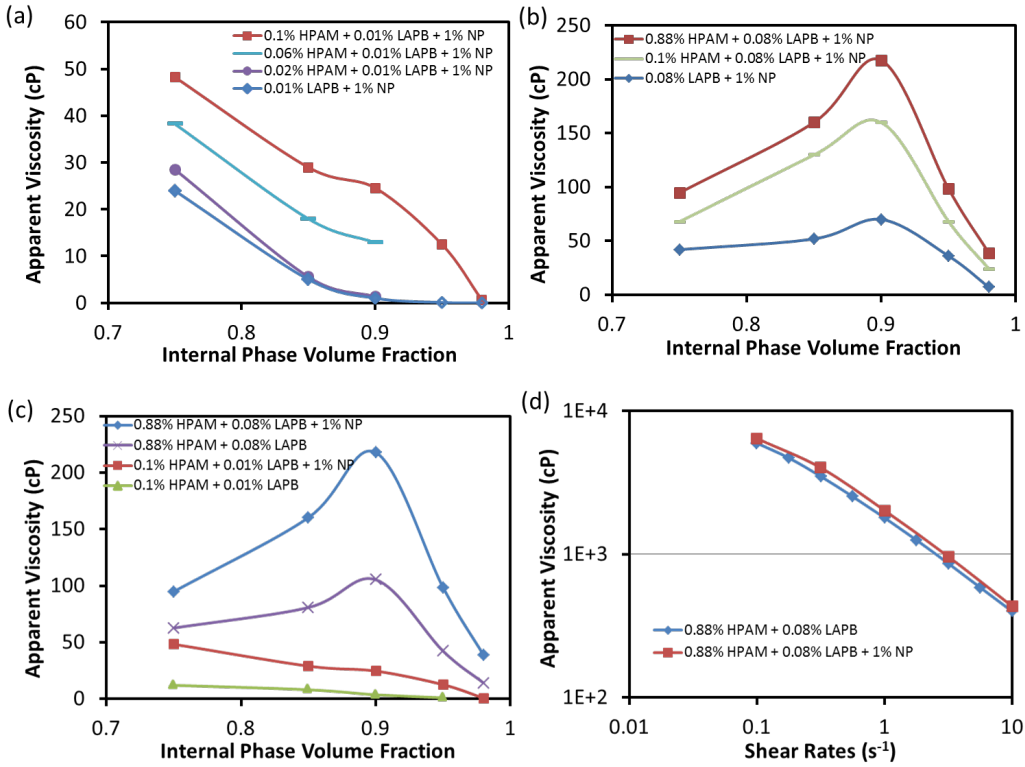
We have developed two different generations of supercritical carbon-dioxide-in-water foams. The first “generation” of such foams [3] had very low water content (2-10% by volume) with the high viscosity on the order of 100cP and long lifetime (hours to days). These foams have been stabilized with either synergistic action of silica nanoparticles lauramidopropyl betaine (LAPB) surfactant and partially hydrolyzed polyacrylamide (HPAM) polymer, see schematic in Figure 4a as opposed to the wormlike micelle formation when (only) viscoelastic surfactants in the second generation of foams are used (Figure 4b).



**Figure 4** Schematic of key mechanisms involved in foam stabilization. (a) Synergy of nanoparticles, polymers and surfactants. (b) Wormlike micelle formation for viscoelastic surfactants.

### 4.2 Foams stabilized with NPs, surfactant and polymer (“the first generation”)

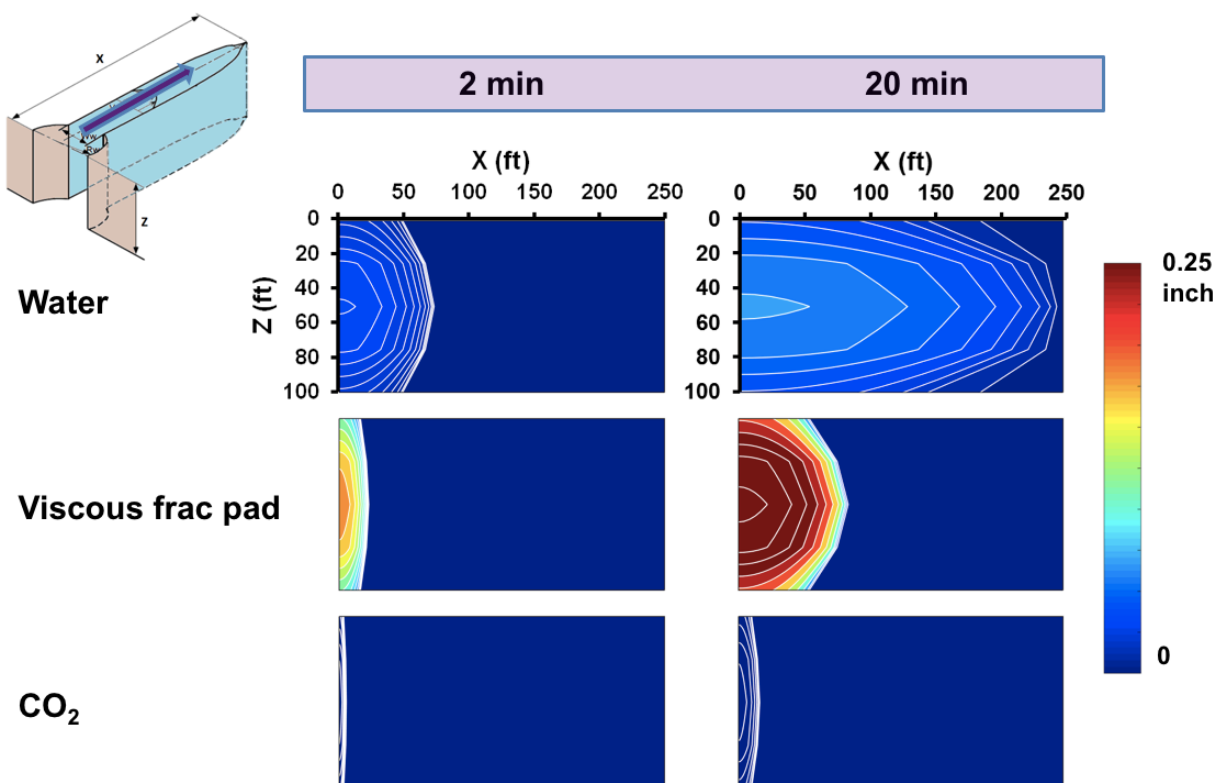
In particular, for the first generation, high continuous phase and surface viscosities produced are a result of opposite charge between surfactant and polymer. CO<sub>2</sub>/brine IFT reduced from 20 mN/m to 5 mN/m at 50 degree Celsius, 3000 psia and up to 2%KCl brine. We saw low lamellae drainage rates and low coalescence, and small bubble size leads to high viscosity of 150-270 cP at 0.90-0.98 quality, at shear rate of 200 s<sup>-1</sup> (Figure 5, also details in [3]). Further, we find that NPs increase the apparent viscosity and stability of foam by reducing Ostwald ripening, and decreasing bubble size by a factor of 2. Finally, NPs irreversibly adsorb to C/W interface, creating an elastic interface. The summary of characterization of these foams are provided in Figure 5.



**Figure 5 (a)-(c) Apparent viscosity of C/W foams in 2 % KCl brine at shear rates of 200 s<sup>-1</sup>, 3000 psi and 50 °C. The concentrations in w/v % are specified in the legend. The lines are only to guide the eyes. (d) The viscosity of the aqueous phase containing mixtures of 0.88% HPAM and 0.08% LAPB, with and without 1% silica NPs. (e)-(j) Micrographs of C/W foams at 3000 psia, 2% KCl brine and room temperature. Scale bar of 100 μm is located in the micrograph. (e)-(g) 90% v/v C/W foams stabilized with mixtures of 0.08% LAPB, 1% NP, and 0, 0.1% and 0.88% HPAM, respectively. (h) 90% v/v C/W foam stabilized with mixtures of 0.08% LAPB and 0.88% HPAM. (i)-(j) 95% v/v C/W foams stabilized with mixtures of 0.88% HPAM, 0.08% LAPB, with and without 1% silica NP.**

## Numerical assessment of fracturing behavior

We have developed a mathematical model to simulate the transport of NP-stabilized foams for hydraulic fracturing [6]. The model combines fluid transport in reservoir matrix and fracture with rock mechanics equations and thus allows for considering the effects of foam on fracture dynamics. Gas and water flow with mechanistic accounting of foam generation and coalescence are simulated using population balance models. Transport of nanoparticles through porous media was simulated using single site filtration model. The equations are discretized using finite-difference scheme. Settari's approach is used to embed fracture's moving boundary with the matrix to accordingly update transmissibility. Model's capabilities are verified with examples on fracture growth and fracture clean up processes to illustrate the benefits of using the NP-stabilized high quality foams. Fracture propagation was simulated for water, a conventional viscous fracpad and NP-stabilized foams of different qualities and textures. The simulations confirmed that larger foam viscosity generated wider fractures with smaller fracture half-length (Figure 6). In addition, fracture cleanup simulations show that fracturing fluid cleanup for foam based fracturing fluids could take the order of 10 days as opposed to that of viscous fracpad which could take up to 1000 days; demonstrating the advantage of using dry foams (Figure 7). More details on the models involved are available in [6].



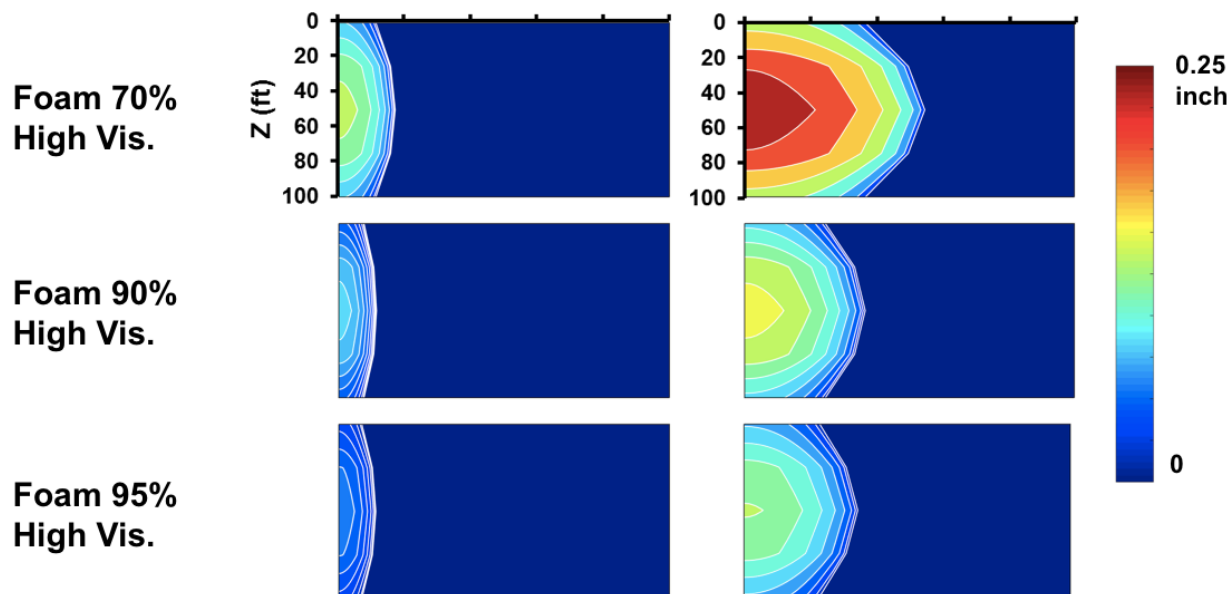


Figure 6 Fracture width and half length for different type of fracturing fluids at two example time steps.

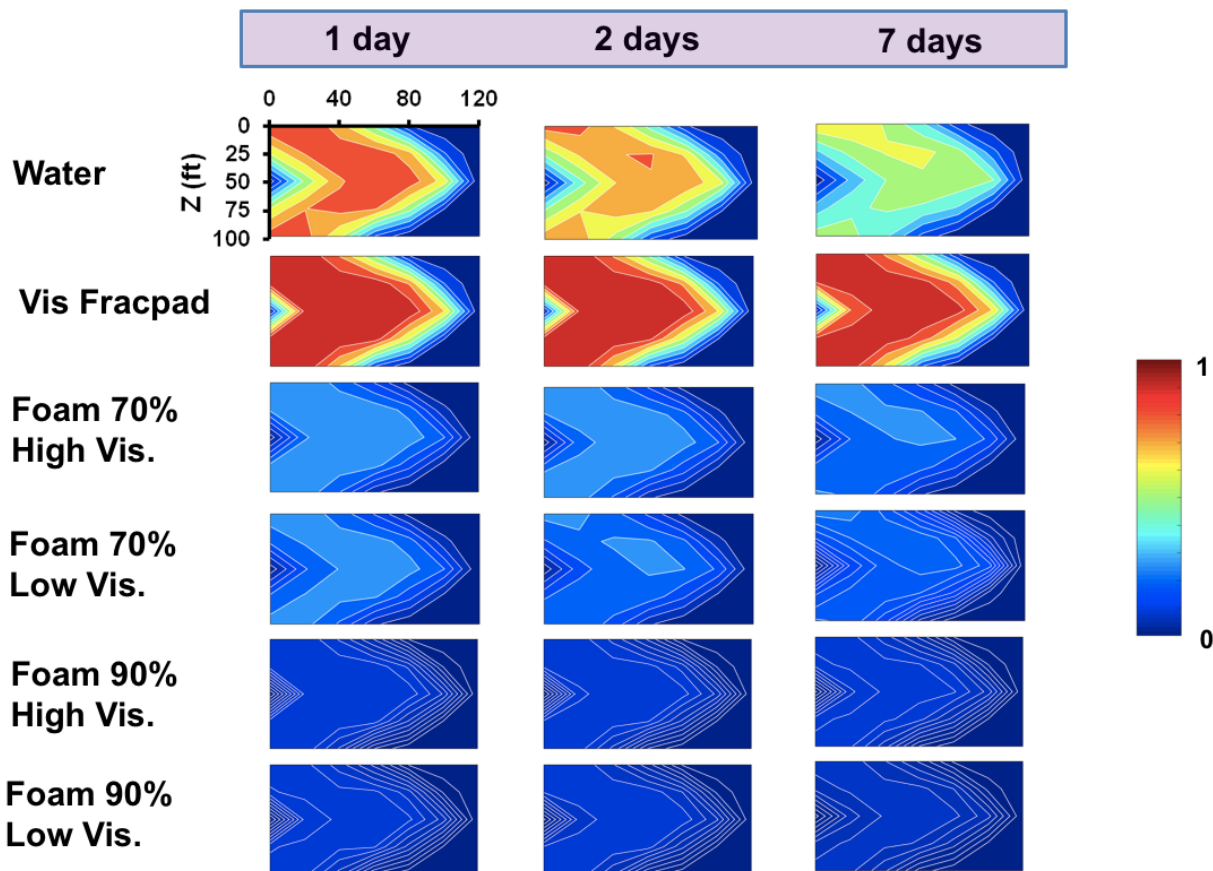
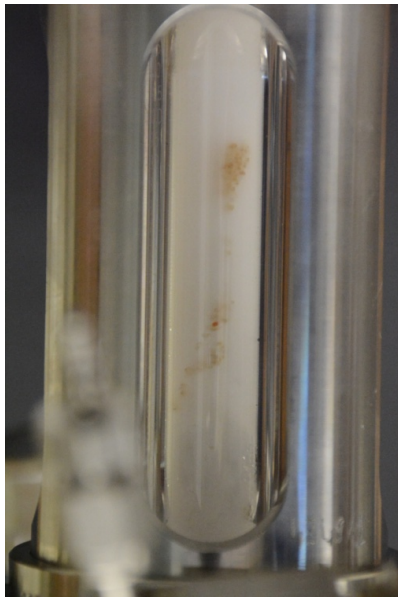


Figure 7 Water saturation (and thus fracture clean-up) at different points in time for different types of fracturing fluids.

## Foam stability test

To verify the stability of the foams they were generated using the pressure loop and then were collected in a sapphire cell at the pressure of 2000 psi, and foam was generated with 90% quality. Bottom of the sapphire cell was coated with sand particles. To evaluate foam viscosity and foam stability, once foam was generated the sapphire cell was inverted and we took image of the sand settling. Within initial seconds, sand particles dropped in the middle of the cell (possibly because of the gas phase gaps in the cell) and once trapped in the foam system, their settling was immediately stopped. Even after one sand particles were trapped in the foam system where they almost did not move. Figure 8 shows the experiment results. Figure 8a was taken at time zero, while Figure 8b was captured after 1 day. As shown in the images, foam density did not visibly changes and sand particles were trapped inside the foam. For more details see [7].



(a)



(b)

**Figure 8: Foam stability test in sapphire cell (a) upon foam generation at time zero and (b) after 1 day. Sand particles are in light brown color.**

## Foam EOR potential evaluation

To evaluate the oil sweeping efficiency upon foam injection into the reservoir, we defined a two-dimensional reservoir, with 27 ft in vertical (z) direction and 100 ft in horizontal (x) direction. Reservoir operating conditions, considered foam properties and other details are

provided in [7]. Here we show the assumed reservoir permeability in Figure 9 as well as the resulting stabilized fluid-fluid front when the foam is used instead of gas in Figure 10.

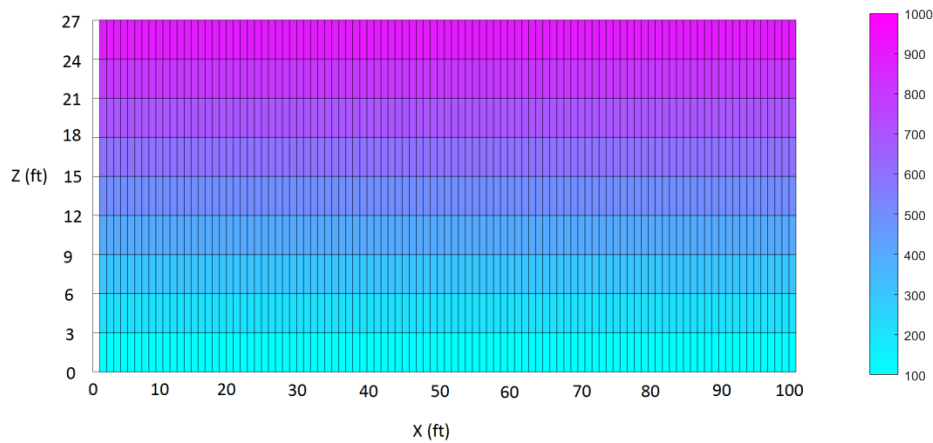


**Figure 9: Layer by layer permeability of the 2D reservoir (mildarcy)**

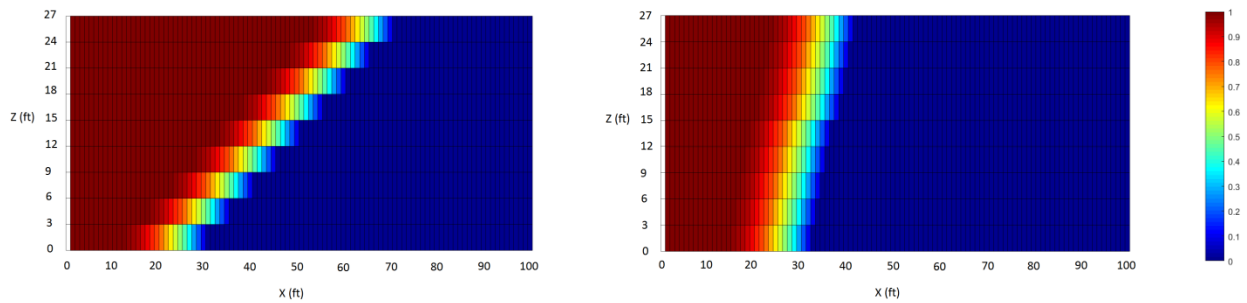


**Figure 10: Side view of normalized  $\text{CO}_2$  concentration at  $\text{PV}=0.4$  for (a) gas-water co-injection (no foam), (b) gas-water co-injection (foam).  $\text{CO}_2$ -water injection (0.9 quality) into the 2D reservoir at rate of 0.365 PV/year. (With no vertical fluid flow consideration).**

### Micromodels experiments (unpublished)

Micromodel experiments reports can be found in Y2Q3 and Y2Q4 quarterly reports. Related network model development can be found in Y2Q4 and Y3Q1 quarterly reports. These preliminary studies that was not planned in the original proposal, and have stopped with the departure of the postdoc working on the project Ali Qajar.

### 4.3 Foams stabilized with viscoelastic surfactants

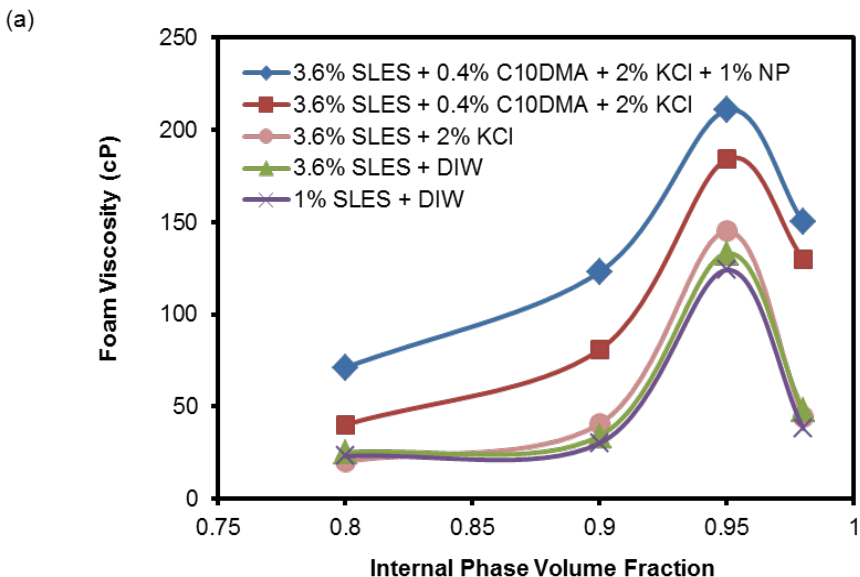
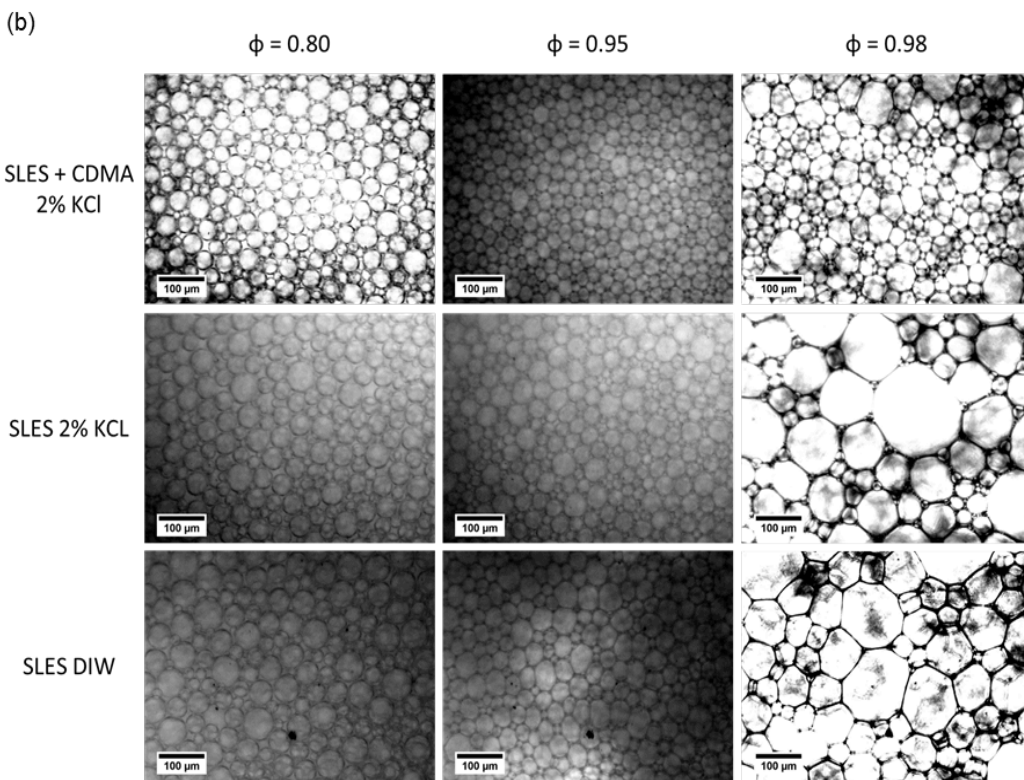


Figure 11 Apparent viscosity of foams stabilized with mixtures of SLES and C<sub>10</sub>DMA at room temperature and 90 °C, 3000 psia, and 190 s<sup>-1</sup> [4].



**Figure 12 Micrographs of foams stabilized with mixtures of SLES and C<sub>n</sub>DMA at room temperature and 90 °C, 3000 psia, and 190 s<sup>-1</sup> [4].**

The second generation of foams is simplified, ultra dry foams formed with sodium lauryl ethoxylated sulfate (SLES) surfactant [4] as well as a series of zwitterionic amidopropylcarbobetaines with more environmentally friendly footprint [5] **without** polymer could potentially be enough to carry out fracturing. The foam is stabilized for up to one day by wormlike micelles formed at low surfactant concentrations as a consequence of their long tails and weak headgroup repulsion. We typically observe high apparent foam viscosity >100 cP at 0.9-0.98 foam quality, temperature up to 90 degrees C, pressure of 3000psi and shear rate of 200 s<sup>-1</sup>, see **Error! Reference source not found.** and Figure 12. The benefit of viscoelasticity is that could potentially allow for more control over triggering destabilization of foams upon depressurization.

Specifically, single zwitterionic surfactants with C<sub>18</sub> or C<sub>22</sub> tails formed wormlike micelles at on 1 wt. % over a wide range of salinity and pH (Figure 13a). We use shortcuts CAPB, OAPB, EAPB that refer to zwitterionic amidopropylcarbobetaine surfactants, R-ONHC<sub>3</sub>H<sub>6</sub>N(CH<sub>3</sub>)<sub>2</sub>CH<sub>2</sub>CO<sub>2</sub>, where R is varied from C<sub>12-14</sub> (coco) to C<sub>18</sub> (oleyl) to C<sub>22</sub> (erucyl). This is substantially lower concentration of surfactants than in the previous work. The concentration range of surfactant ultra-dry foams with up to 98% CO<sub>2</sub> by volume has been lowered to only 1% in the aqueous phase with single zwitterionic amidopropylcarbobetaine zwitterionic surfactants that are commercially available. Using the same surfactants, the temperature range of ultra-dry foams has been extended up to 120 degrees C (Figure 13b).The foams are stabilized despite the high temperature by the same mechanism of formation of wormlike micelles that slow down the drainage of the aqueous lamellae between the foam bubbles.

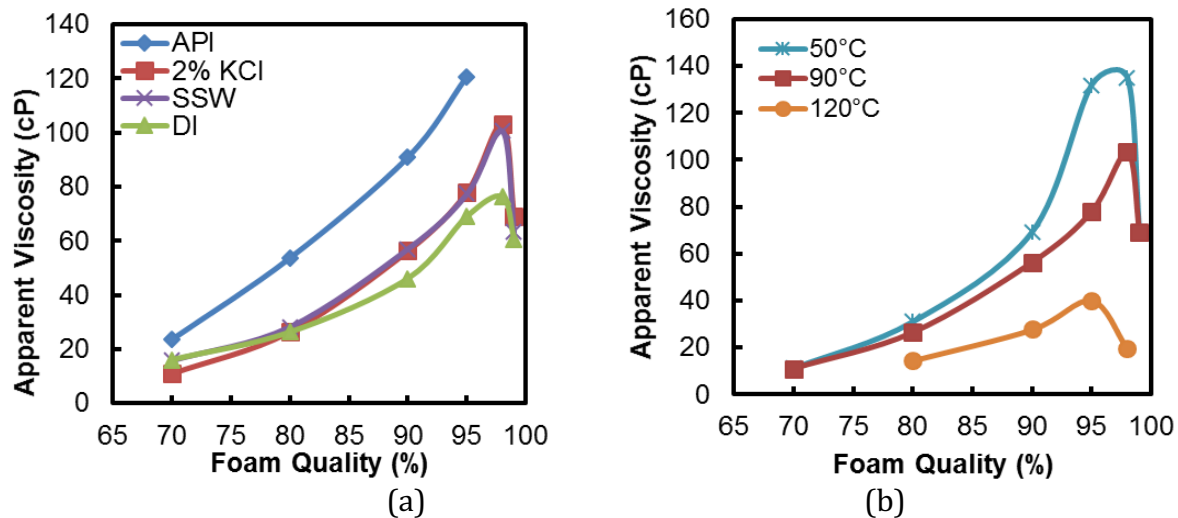


**Figure 13 Apparent viscosity of foams stabilized with 1% wt. C<sub>n</sub>amidopropylbetaine surfactant**

**at shear Rate of 200 s<sup>-1</sup> and 3000 psig. a) Salt effect at 90 degrees C and (b) Temperature effect at 2% KCl.**

Long term stability is dominated by Ostwald ripening and it is decreased 30-fold upon formation of wormlike micelles. We observe the slowest Ostwald ripening for C<sub>22</sub> - mean bubble diameter for various cases is shown in **Figure 14**.

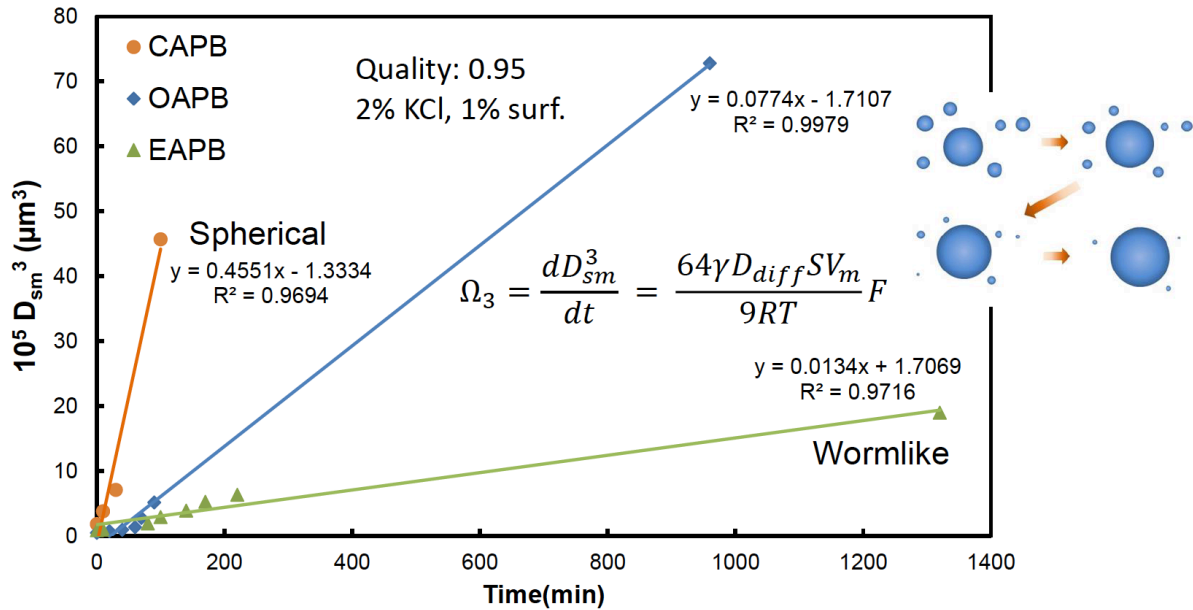


**Figure 14** Static C/W foam stability in terms of  $D_{sm}$  versus time for 1% surfactant in 2% KCl brine at 25 °C, 3000 psig, and 0.95 quality.

#### 4.4. Nitrogen-in-water foams (unpublished)

We are investigating repeatability of the CO<sub>2</sub> foam results with N<sub>2</sub>. Foam stability and rheology are investigated for different foam quality and for elevated temperatures. Foam stability at high temperature is not given and takes experimentation with the right surfactants. Thus until the investigation is complete and ready for publishing, we are referring to the surfactant we found working well as “Surfactant F”.

The texture of foams generated by flowing N<sub>2</sub> and brine/surfactant mixture through two different bead packs (of 22D and 1.8D permeability respectively) is shown in Figure 15. Brine salinity was 2% KCl, and surfactant concentration was 1%. Figure 16 and Figure 17 show apparent viscosity for different foam texture and different temperatures, respectively.

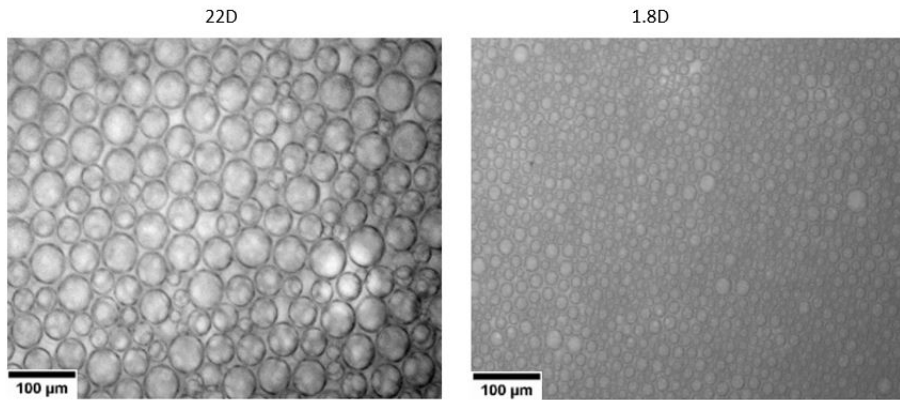


**Figure 15** Foam texture for N2 foam generated with two different bead packs (of 22D and 1.8D permeability respectively).

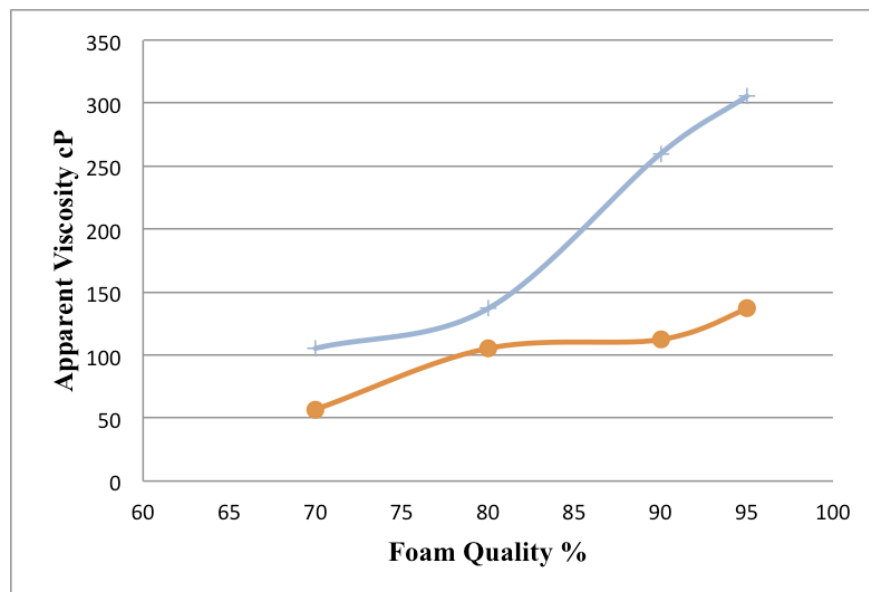


**Figure 16** Apparent foam viscosity at the shear rate of 200s<sup>-1</sup>. Blue curve is viscosity of the foam with smaller bubble size (finer texture, created with 1.8D bead pack), and the lower curve is corresponding to the foam with the coarser texture.

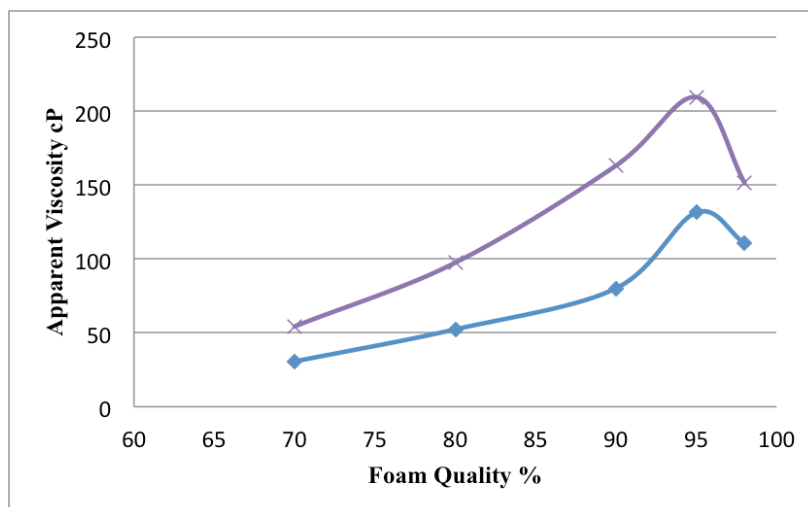


**Figure 17 Apparent viscosity of the nitrogen foam for the coarser texture, 1% surfactant concentration, shear rate 200s-1. The upper and lower curve correspond to 50 and 90 degrees Celsius, respectively.**

We have the following publication in preparation: S. Alzobaidi, C. Da, M. Prodanović, and K. P. Johnston, “High temperature high pressure ultra-dry nitrogen-in-water foams”

#### **4.5 Further study on the effect of nanoparticles in foam (unpublished)**

Whereas many studies have examined stabilization of emulsions and foams in low salinity aqueous phases with nanoparticles (NPs) with and without added surfactants, interest has grown recently in much higher salinity brines relevant to subsurface oil and gas applications. We hypothesize that the synergy of nanoparticles and surfactants will enable stable foams in conditions harsher than previously investigated.

We report stabilization of foams at high salinity where the aqueous phase is API brine, 8% NaCl and 2% CaCl<sub>2</sub> with a combination of nanoparticles (NPs) and surfactant that exhibit synergies with regard to both foam generation and stabilization. The nanoparticles were synthesized in our lab, and the surfactant has not been previously used. Until we collect more data, we refer to them as nanoparticles K.



**Figure 18 Schematic showing surfactant adsorption to the surface of NPs and resulting change in CO<sub>2</sub>-philicity.**

When either NPs or surfactant alone are used to generate foam, very weak foam is formed with an apparent foam viscosity of less than 4 cP. However, with mixtures of nanoparticles and surfactants over the same concentration range, the apparent foam viscosity reached 60 centipoise. The benefit of surfactants is that they lower the interfacial tension more effectively, and the benefit of nanoparticles is that they adsorb more irreversibly at the water-CO<sub>2</sub> interface (see Figure 18). These results provide a basis for future studies of the mechanism of foam formation

and stabilization with NPs and NP/surfactant mixtures at high salinity and for development of practical applications of nanoparticle stabilized fracture fluids.

The concentration of NPs and surfactant in solutions ranged from 0.1% NPs and 0.01% surfactant to 1% NPs and 0.1% surfactant. As shown in Figure 19, the initial foam bubble size at 70% quality increased as the concentrations of surfactant and NPs increased to 1% NPs and 0.1% surfactant at 25°C. Initial foam bubble size at 80°C was greater than 100 micron until the mixture concentration reached 0.7% NPs and 0.07% surfactant. At 80°C, we notice there is a surfactant threshold concentration between 0.05% surfactant and 0.07% surfactant resulting in the generation of foam bubbles less than 100 micron.

The apparent foam viscosities generated at 25°C ranged from 3 cP to 65 cP, Figure 20(A). The apparent foam viscosity at 70% and 80% quality reached a plateau of 51 cP starting at 0.5% NPs and 0.05% surfactant. However, apparent foam viscosities at 90% quality kept rising with an increase in the concentrations of NPs and surfactant. At high concentrations, a greater amount of surfactant and NPs exist in the lamella which help balance the disjoining pressure against the capillary pressures.

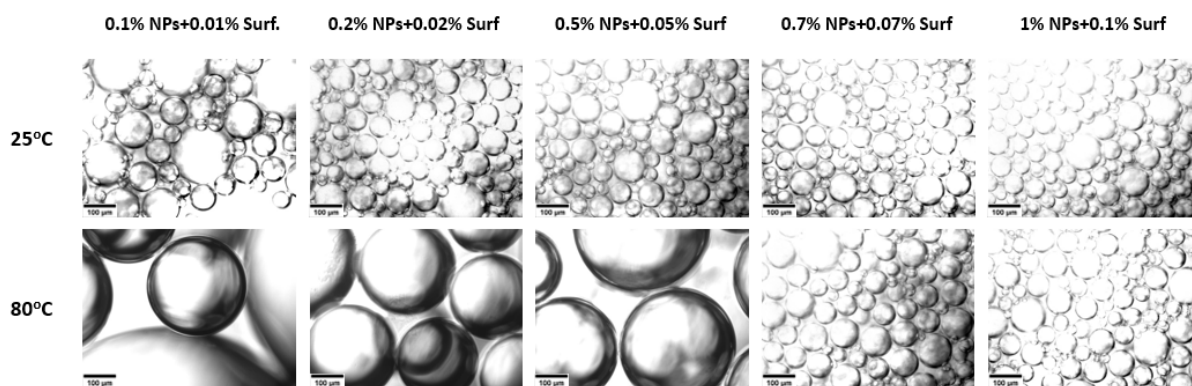


**Figure 19 Micrographs for foam generated with surfactant and NPs in API brine at different concentrations shown above at 70 quality and 3000 psig.**

When the temperature was increased to 80°C, the apparent foam viscosity for the same concentrations ranged from 0.6 cP to 41 cP, Figure 20(B). The apparent foam viscosity at 70% quality and 80% quality reached a plateau at 0.7% NPs and 0.07% surfactant. Similar to the 25°C foam generation experiments, the apparent foam viscosity of 90% quality foam kept rising as the concentration of NPs and surfactant increased. At high temperatures, we anticipate that the interfacial tension is higher based on our previous studies and thus the capillary pressure is greater, which leads to foam destabilization. Lower apparent foam viscosity at 80°C can also be attributed to more rapid CO<sub>2</sub> diffusion that at lower temperature. The more rapid diffusion would increase the rate of Ostwald ripening and increase the bubble sizes, as observed, which would be consistent with the reduction in foam viscosities.

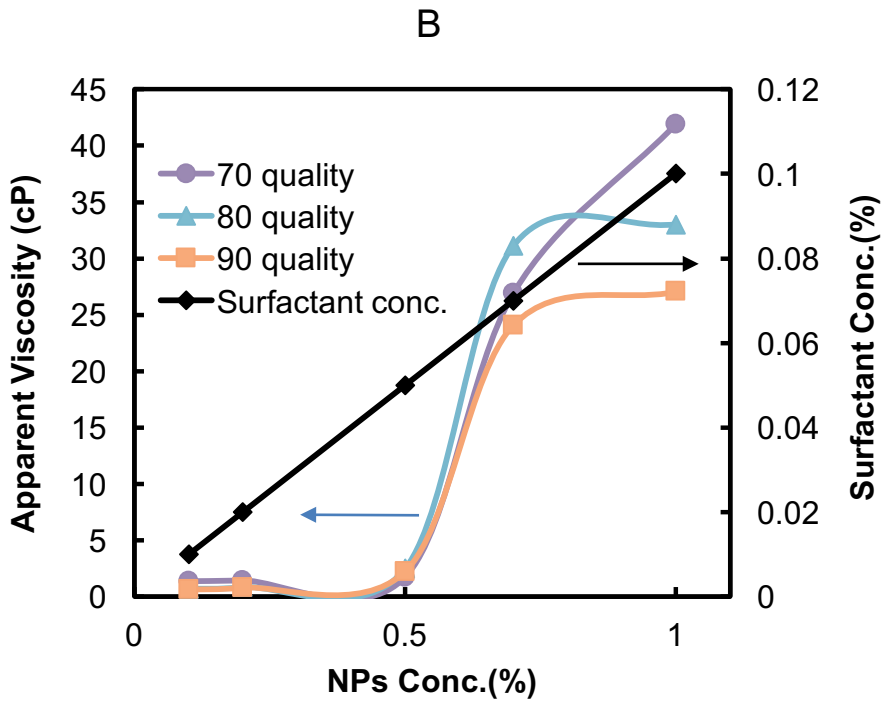
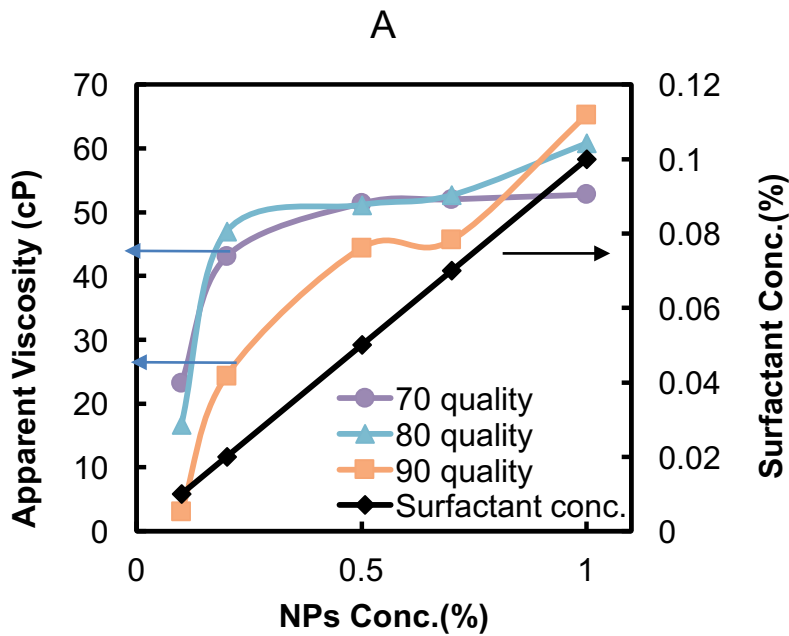


**Figure 20** Apparent CO<sub>2</sub>/brine foam viscosity vs. foam quality for various NP and surfactant concentrations in the continuous API brine phase. The foams were generated in a 22 Darcy bead pack at 3000 psig and a shear rate of 750 s<sup>-1</sup> at A) 25 degrees C B) 80 degrees C.

We finally describe three types of surface modified nanoparticles, low surface modification LC, medium surface modification MC, and high surface modification HC. All the nanoparticles were

obtained from a commercial source so we do not know the details on surface modification. For foam generated with nanoparticles at 25°C, the apparent foam viscosity reached > 35 cP at a quality of 85%. However, the apparent foam viscosity decreased with decreasing the coverage on the surface of the nanoparticles, Figure 21.

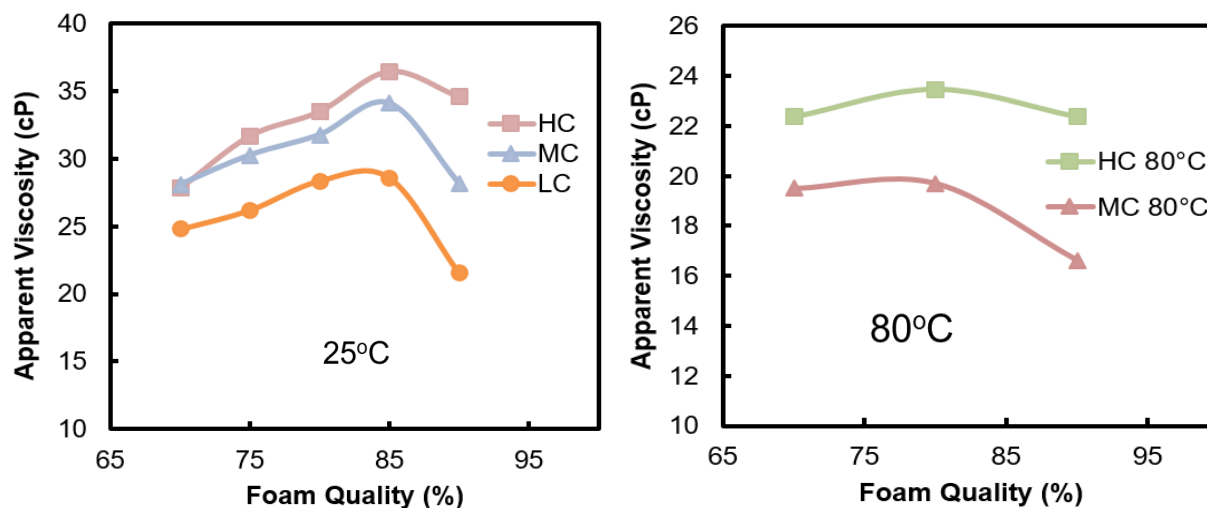


Figure 21 Apparent foam viscosity vs foam quality LC, MC, and HC modified NPs in a 22Darcy beadpack at 3000 psig and 750 s-1.

At high temperature of 80°C the LC NPs lost colloidal stability and were not tested. However, HC and MC NPs were stable and an apparent foam viscosity of 24 cP was achieved with HC NPs. We expect HC NPs to adsorb more to the interface. We are currently investigating the role of the surface chemistry of the nanoparticles to better understand how the foam texture and rheological properties change with foam quality. Our preliminary evidence suggests that the greater adsorption of HC at the CO<sub>2</sub>-water interface may be beneficial relative to MC for foam stabilization at high qualities at high temperature. This observation was also true for long term stability at room temperature where HC NP foam had the best stability compared to LC and MC foam, Figure 22.

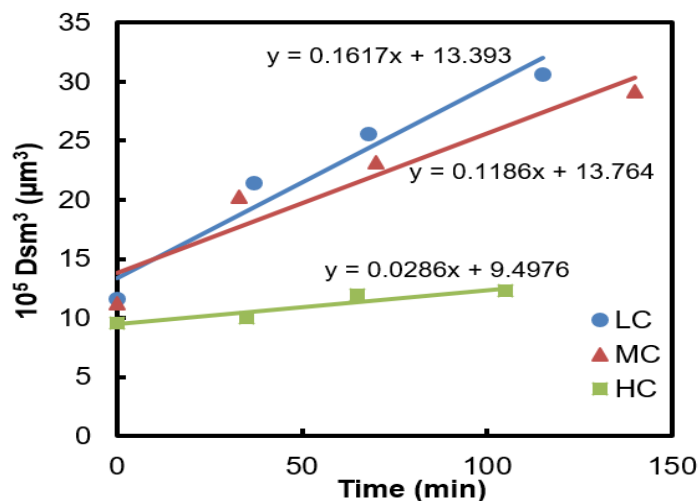


Figure 22 Long term stability for LC, MC, and HC NPs generated in a 22-Darcy beadpack at 3000 psig and 750 s<sup>-1</sup> at room temperature.

#### 4.6. Publications from this work

We do not include copies of the final versions of the published papers as they are available at the appropriate journal websites.

##### Peer reviewed journal publications:

1. Z. Xue, A. Worthen, A. Qajar, I. Robert, S. L. Bryant, C. Huh, M. Prodanović, and K. P. Johnston, "Viscosity and stability of ultra-high internal phase CO<sub>2</sub>-in-water foams stabilized with surfactants and nanoparticles with or without polyelectrolytes," *Journal of Colloid and Interface Science*, vol. 461, pp. 383–395, Jan. 2016.
2. Z. Xue, A. J. Worthen, C. Da, A. Qajar, I. R. Ketchum, S. Alzobaidi, C. Huh, M. Prodanović, and K. P. Johnston, "Ultradry Carbon Dioxide-in-Water Foams with Viscoelastic Aqueous Phases," *Langmuir*, vol. 32, no. 1, pp. 28–37, Jan. 2016.
3. A. Qajar, Z. Xue, A. J. Worthen, K. P. Johnston, C. Huh, S. L. Bryant, and M. Prodanović, "Modeling fracture propagation and cleanup for dry nanoparticle-stabilized-foam fracturing fluids," *Journal of Petroleum Science and Engineering*, vol. 146, pp. 210–221, Oct. 2016.
4. S. Alzobaidi, C. Da, V. Tran, M. Prodanović, and K. P. Johnston, "High temperature ultralow water content carbon dioxide-in-water foam stabilized with viscoelastic zwitterionic surfactants," *Journal of Colloid and Interface Science*, vol. 488, pp. 79–91, Feb. 2017.

##### Journal publications in preparation:

5. S. Alzobaidi, C. Da, M. Prodanović, and K. P. Johnston, "High temperature high pressure ultra-dry nitrogen-in-water foams", in preparation

**Conference paper:**

1. C. Da, Z. Xue, A. J. Worthen, A. Qajar, C. Huh, M. Prodanovic, and K. P. Johnston, "Viscosity and Stability of Dry CO<sub>2</sub> Foams for Improved Oil Recovery," in *SPE Improved Oil Recovery Conference Proceedings*, Tulsa, OK, 2016, Paper number 179690.

**PhD Thesis:**

1. Zheng Xue, "[Stability and rheology of high internal phase CO<sub>2</sub>-in-water foams and stability and transport of polymer grafted nanoparticles](#)", PhD Thesis, The University of Texas at Austin, 2015

**Public/recorded webinar:**

1. "Recent advances in subsurface foam applications", M. Prodanović, Q. Nguyen and K. Johnston, Knowledge Pipeline Webinar, Center for Petroleum and Geosystems Engineering, UT Austin, May 12, 2017, available on <https://meeting.austin.utexas.edu/p6cmt7izezy/?launcher=false&fcsContent=true&pbMode=normal>

## 5 Conclusions

This project demonstrated that suitably coated nanoparticles or viscoelastic surfactants can stabilize foams of fluids potentially useful for hydraulic fracturing at elevated pressures and at temperatures ranging from ambient to reservoir conditions. The water-based foams require four to twenty times less water per barrel of fluid than conventional water-based fracturing fluids. Thus, this research could have a significant impact on the development of unconventional oil and gas resources in areas where water use and/or disposal is constrained.

The results of this research expand the options available to operators for hydraulic fracturing and can simplify the design and field implementation of foamed fracturing fluids. The technology will make it easier for operators to switch to reduced-water or zero-water hydraulic fracturing campaigns, thereby alleviating one of the most sensitive challenges for domestic hydrocarbon production.

There is great momentum in both lab- and field-scale work, but further research is needed to fully:

1. Fundamentally understand and describe (develop models on) the viscosity and stability of these foams based on the properties of the stabilizers and describe their behavior in in-situ conditions both as bulk foam (i.e. flowing through geometries much larger than the foam bubble size) as well as in porous media/fractures (of pore size/apertures similar to the bubble size).
2. Investigate nitrogen or methane as gas phase in addition to CO<sub>2</sub> and compare their efficacies. Compressible gases, for instance, might be beneficial in depressurization-triggered foam break-down during clean-up. Show experimentally foam stability versus surfactant structure and interfacial properties.
3. Investigate field application of the new ultra-dry foams.

## 6 List of Figures

Figure 1 The overview of the synergy required for stabilization of ultradry foams as well as their intended usage in hydraulic fracturing. Ultradry foams are defined as foams with volumetric gas content, or quality, of 90% and above.....	4
Figure 2 Schematic of ultradry foams gas content vs. the hydraulic fracturing fluids currently in use (a) water, (b) energized fluids (gas content $Q \sim 0.3$ ), (c) foam ( $Q \sim 0.6$ ), and (d) ultrdry foam ( $Q > 0.9$ ).....	5
Figure 3. Schematic of the apparatus used for apparent foam viscosity and mean bubble size measurements. A glass bead pack was used as the foam generator.....	8
Figure 4 Schematic of key mechanisms involved in foam stabilization. (a) Synergy of nanoparticles, polymers and surfactants. (b) Wormlike micelle formation for viscoelastic surfactants. ....	10
Figure 5 (a)-(c) Apparent viscosity of C/W foams in 2 % KCl brine at shear rates of 200 $s^{-1}$ , 3000 psi and 50 °C. The concentrations in w/v % are specified in the legend. The lines are only to guide the eyes. (d) The viscosity of the aqueous phase containing mixtures of 0.88% HPAM and 0.08% LAPB, with and without 1% silica NPs. (e)-(j) Micrographs of C/W foams at 3000 psia, 2% KCl brine and room temperature. Scale bar of 100 $\mu m$ is located in the micrograph. (e)-(g) 90% v/v C/W foams stabilized with mixtures of 0.08% LAPB, 1% NP, and 0, 0.1% and 0.88% HPAM, respectively. (h) 90% v/v C/W foam stabilized with mixtures of 0.08% LAPB and 0.88% HPAM. (i)-(j) 95% v/v C/W foams stabilized with mixtures of 0.88% HPAM, 0.08% LAPB, with and without 1% silica NP. ....	11
Figure 6 Fracture width and half length for different type of fracturing fluids at two example time steps.....	13
<b>Figure 7 Water saturation (and thus fracture clean-up) at different points in time for different types of fracturing fluids.....</b>	<b>13</b>
<b>Figure 8: Foam stability test in sapphire cell (a) upon foam generation at time zero and (b) after 1 day. Sand particles are in light brown color. ....</b>	<b>14</b>
Figure 9: Layer by layer permeability of the 2D reservoir (mildarcy).....	15
Figure 10: Side view of normalized $CO_2$ concentration at $PV=0.4$ for (a) gas-water co-injection (no foam), (b) gas-water co-injection (foam). $CO_2$ -water injection (0.9 quality) into the 2D reservoir at rate of 0.365 PV/year. (With no vertical fluid flow consideration).....	15
Figure 11 Apparent viscosity of foams stabilized with mixtures of SLES and $C_{10}DMA$ at room temperature and 90 °C, 3000 psia, and 190 $s^{-1}$ [4].....	16
Figure 12 Micrographs of foams stabilized with mixtures of SLES and $C_{10}DMA$ at room temperature and 90 °C, 3000 psia, and 190 $s^{-1}$ [4]. ....	17
Figure 13 Apparent viscosity of foams stabilized with 1% wt. $C_{18}$ amidopropylbetaine surfactant.....	17
<b>Figure 14 Static C/W foam stability in terms of <math>D_{sm}</math> versus time for 1% surfactant in 2% KCl brine at 25 °C, 3000 pisp, and 0.95 quality.....</b>	<b>18</b>
Figure 15 Foam texture for $N_2$ foam generated with two different bead packs (of 22D and 1.8D permeability respectively).....	19
Figure 16 Apparent foam viscosity at the shear rate of 200 $s^{-1}$ . Blue curve is viscosity of the foam with smaller bubble size (finer texture, created with 1.8D bead pack), and the lower curve is corresponding to the foam with the coarser texture.....	19

Figure 17 Apparent viscosity of the nitrogen foam for the coarser texture, 1% surfactant concentration, shear rate 200s-1. The upper and lower curve correspond to 50 and 90 degrees Celsius, respectively.....	20
Figure 18 Schematic showing surfactant adsorption to the surface of NPs and resulting change in CO <sub>2</sub> -philicity.....	20
Figure 19 Micrographs for foam generated with surfactant and NPs in API brine at different concentrations shown above at 70 quality and 3000 psig.....	21
Figure 20 Apparent CO <sub>2</sub> /brine foam viscosity vs. foam quality for various NP and surfactant concentrations in the continuous API brine phase. The foams were generated in a 22 Darcy bead pack at 3000 psig and a shear rate of 750 s <sup>-1</sup> at A) 25 degrees C B) 80 degrees C.....	22
Figure 21 Apparent foam viscosity vs foam quality LC, MC, and HC modified NPs in a 22Darcy beadpack at 3000 psig and 750 s-1.....	23
Figure 22 Long term stability for LC, MC, and HC NPs generated in a 22-Darcy beadpack at 3000 psig and 750 s <sup>-1</sup> at room temperature.....	24

## 7 List of Tables

Table 1. Summary of ultra dry CO <sub>2</sub> /water foam systems. These are representative systems rather than an exhaustive list (please refer to publications).....	6
--	---

## 8 References

- [1] R. E. Blauer and C. A. Kohlhaas, "Formation Fracturing with Foam," presented at the Fall Meeting of the Society of Petroleum Engineers of AIME, 1974.
- [2] G. E. King, "Foam and Nitrified Fluid Treatments-Stimulation Techniques and More," Jan. 1985.
- [3] Z. Xue *et al.*, "Viscosity and stability of ultra-high internal phase CO<sub>2</sub>-in-water foams stabilized with surfactants and nanoparticles with or without polyelectrolytes," *J. Colloid Interface Sci.*, vol. 461, pp. 383–395, Jan. 2016.
- [4] Z. Xue *et al.*, "Ultradry Carbon Dioxide-in-Water Foams with Viscoelastic Aqueous Phases," *Langmuir*, vol. 32, no. 1, pp. 28–37, Jan. 2016.
- [5] S. Alzobaidi, C. Da, V. Tran, M. Prodanović, and K. P. Johnston, "High temperature ultralow water content carbon dioxide-in-water foam stabilized with viscoelastic zwitterionic surfactants," *J. Colloid Interface Sci.*, vol. 488, pp. 79–91, Feb. 2017.
- [6] A. Qajar *et al.*, "Modeling fracture propagation and cleanup for dry nanoparticle-stabilized-foam fracturing fluids," *J. Pet. Sci. Eng.*, vol. 146, pp. 210–221, Oct. 2016.
- [7] C. Da *et al.*, "Viscosity and Stability of Dry CO<sub>2</sub> Foams for Improved Oil Recovery," in *SPE Improved Oil Recovery Conference Proceedings*, Tulsa, OK, 2016, p. Paper number 179690.
- [8] G. Beck *et al.*, "Laboratory Evaluation of a Natural Gas-Based Foamed Fracturing Fluid," in *SPE Annual Technical Conference and Exhibition Proceedings*, 2017, p. Paper number 187199.